UNIVERSITY
OF TRENTO

DEPARTMENT OF INFORMATION AND COMMUNICATION TECHNOLOGY

38050 Povo – Trento (Italy), Via Sommarive 14
http://www.dit.unitn.it

A SIMPLE FDTD MODEL TO ASSES THE FEASIBILITY OF HEART BEAT
DETECTION USING COMMERCIAL UWB COMMUNICATION DEVICES

Carlos Bilich
www.carlosbilich.com.ar

January 4th, 2007

A Simple FDTD Model to Asses the Feasibility of Heart Beat Detection using commercial UWB communication devices

Carlos G. Bilich

Abstract. This work studies the propagation and the attenuation suffered by an UWB impulse on its way to the human heart traveling through the chest. The latter is modeled as multiple semi-infinite lossy and dispersive media. The radiated impulse is a Gaussian monocycle similar to those used in UWB communications. The formulation uses the FDTD method to approximate the solution of the Maxwell's equations. The results show that the chest attenuates the impulse approximately 42dB which is significantly lower than the values predicted by previous approximations. This would eventually improve the performance and range of UWB vital signs sensing applications.

1 Introduction

In previous works, (i.e Bilich [4],[5],[6] and [10]), the estimation of the attenuation suffered by an UWB impulse as it crosses the chest tissues was done in the far field using the well known Friis formula. However, it was then argued that was only a coarse approximation, because for the distances and dimensions being considered, only a full wave analysis could give more reliable results. This work is a step forward towards this objective. This is the first of a series of projected articles in which the Maxwell's curl equations will be solved directly to study the propagation of the impulse. The technique chosen is the Finite Differences Time Domain (FDTD) method of proved efficacy for the solution of similar problems in computational electromagnetics. The approach follows the one of Sullivan's book [1], that starts posing the problem in one dimension to further increase the complexity up to three dimensions. Therefore, this article starts formulating the problem in one dimension. However, in spite of its simplicity the results obtained are very useful to demonstrate the viability of going forward towards this research path and to encourage the effort that would signify going for more dimensions.

Specifically this work uses a one dimensional FDTD simulation to asses the propagation performance in tissues of the Gaussian monocycle proposed for UWB communications. This is of particular interest to build devices that can do both: communications and sensing with the same UWB transceiver.

The Friis expression used previously gives the result only for one particular frequency. However, the short duration of the impulses considered here makes them inherently ultra wideband. The solution would have required a differential formulation of the Friis formula to be later on integrated throughout the whole bandwidth of interest. This approach, though, would still have suffered from the fact that it is only valid in the far field.

By using the FDTD simulation it was possible to confirm the superior performance of the Gaussian monocycle to go through the tissues and come back with a significant lower attenuation than what was predicted by the monofrequency analysis. This is very important considering the extremely low power envisioned for UWB communications and medical monitoring devices as regulated by the FCC [2].

2 One dimensional FDTD formulation

The Maxwell's curl equations for nonmagnetic source-free regions can be written as:

$$\frac{\partial \mathbf{D}}{\partial t} = \nabla \times \mathbf{H}$$

$$\frac{\partial \mathbf{H}}{\partial t} = -\frac{1}{\mu_0} \nabla \times \mathbf{E}$$

where

$\quad$ **D**: Electric flux density vector [Coulombs/m^2]
$\quad$ **E**: Electric field intensity vector [V/m]
$\quad$ **H**: Magnetic field intensity vector [A/m]
$\quad$ μ_0: Free space permeability = 4π x 10^{-7} [H/m]
in particular:

$$\mathbf{D} = \mathbf{D}(\omega) = \varepsilon_0 \cdot \varepsilon_r^*(\omega) \cdot \mathbf{E}(\omega)$$

where

$\quad \varepsilon_0 \qquad$ Free space permittivity = 8.854 x 10^{-12} [F/m]
$\quad \varepsilon_r^*(\omega) \qquad$ Frequency dependant complex relative dielectric constant

$\omega = 2\pi f$ Angular frequency [rad/s]

f Frequency [Hz]

To simplify the formulation of the FDTD equations, it is better to express the Maxwell's equations using normalized Gaussian units by substituting [1]:

$$\widetilde{\mathbf{E}} = \sqrt{\frac{\varepsilon_0}{\mu_0}} \cdot \mathbf{E} \; ; \qquad \widetilde{\mathbf{D}} = \sqrt{\frac{1}{\varepsilon_0 \cdot \mu_0}} \cdot \mathbf{D}$$

which leads to:

$$\frac{\partial \widetilde{\mathbf{D}}}{\partial t} = \frac{1}{\sqrt{\varepsilon_0 \mu_0}} \nabla \times \mathbf{H}$$

$$\frac{\partial \mathbf{H}}{\partial t} = -\frac{1}{\sqrt{\varepsilon_0 \mu_0}} \nabla \times \widetilde{\mathbf{E}}$$

$$\widetilde{\mathbf{D}}(\omega) = \varepsilon_r^*(\omega) \cdot \widetilde{\mathbf{E}}(\omega)$$

Assuming a plane wave with the electric field oriented in the x direction, the magnetic field oriented in the y direction, and traveling in the z direction; in one dimension the equations reduce to:

$$\frac{\partial \widetilde{D}x}{\partial t} = -\frac{1}{\sqrt{\varepsilon_0 \mu_0}} \frac{\partial Hy}{\partial z}$$

$$\frac{\partial Hy}{\partial t} = -\frac{1}{\sqrt{\varepsilon_0 \mu_0}} \frac{\partial \widetilde{E}x}{\partial z} \tag{1}$$

$$\widetilde{D}x(\omega) = \varepsilon_r^*(\omega) \cdot \widetilde{E}x(\omega)$$

Before taking the finite difference approximation of the above expressions, let's define an interleaved one dimensional FDTD grid as showed in Fig. 1:
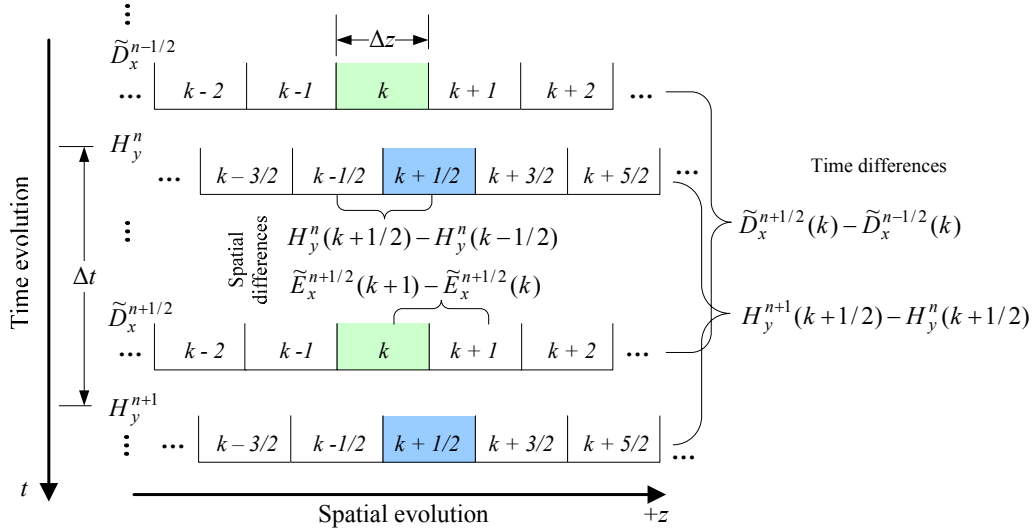

Fig. 1. FDTD interleaving grid showing the interdependence between the $\widetilde{E}x$, $\widetilde{D}x$ and Hy fields; k is the distance counter such that the total simulated distance is $z = k \cdot \Delta z$, and n is the time counter such that the total simulated time is $t = n \cdot \Delta t$; where Δz and Δt stand for cell size and the time step respectively.

Based on that grid, the central difference approximations for both the temporal and spatial derivatives can be written as:

$$\frac{\widetilde{D}_x^{n+1/2}(k) - \widetilde{D}_x^{n-1/2}(k)}{\Delta t} = -\frac{1}{\sqrt{\mu_0 \varepsilon_0}} \frac{H_y^n(k+1/2) - H_y^n(k-1/2)}{\Delta z}$$

$$\frac{H_y^{n+1}(k+1/2) - H_y^n(k+1/2)}{\Delta t} = -\frac{1}{\sqrt{\mu_0 \varepsilon_0}} \frac{\widetilde{E}_x^{n+1/2}(k+1) - \widetilde{E}_x^{n+1/2}(k)}{\Delta z}$$

Rearranging them for their implementation as an iterative algorithm:

$$\widetilde{D}_x^{n+1/2}(k) = \widetilde{D}_x^{n-1/2}(k) - \frac{1}{\sqrt{\mu_0 \varepsilon_0}} \frac{\Delta t}{\Delta z} \left[H_y^n(k+1/2) - H_y^n(k-1/2) \right] \tag{2}$$

$$H_y^{n+1}(k+1/2) = H_y^n(k+1/2) - \frac{1}{\sqrt{\mu_0 \varepsilon_0}} \frac{\Delta t}{\Delta z} \left[\widetilde{E}_x^{n+1/2}(k+1) - \widetilde{E}_x^{n+1/2}(k) \right]$$

To determine the time step Δt it must be taken into account that an electromagnetic wave propagating in free space cannot go faster than the speed of light, thus to propagate a distance of one cell requires a minimum time of $\Delta t = \Delta z/c_0$. This is just the special case of a more general expression known as the "Courant Condition", which establishes that for n dimensions: $\Delta t \leq \Delta z/\left(\sqrt{n} \cdot c_0\right)$. For simplicity, the value adopted here is:

$$\Delta t = \frac{\Delta z}{2 \cdot c_0} \tag{3}$$

This condition works also well when the propagation speed $v < c_0$, and thus $\Delta t < \Delta t_v = \Delta z/(2 \cdot v)$, which assures also good accuracy in slower mediums such as the tissues that make up the chest.
Therefore using expression (3),

$$\frac{1}{\sqrt{\mu_0 \varepsilon_0}} \frac{\Delta t}{\Delta z} = c_0 \cdot \frac{\Delta z/(2 \cdot c_0)}{\Delta z} = \frac{1}{2}$$

Rewriting eqs. (2) for their implementation in C computer code gives:

```
dx[k] = dx[k] - 0.5*( hy[k] - hy[k-1] );
hy[k] = hy[k] - 0.5*( ex[k+1] - ex[k] );
```

Superscripts n, $n+1/2$ and $n-1/2$ are gone because time is implicit in the FDTD method, and the location respect to equal sign indicates what is the actual and the previous value. Spatial position, however, is explicit, and in order to use a computer array, $k+1/2$ and $k-1/2$ have been rounded of to k and $k-1$ respectively. In the computer program, the space interleaving effect, is achieved by shifting the ranges of the `for` loops that compute `dx` and `hy`.

3   Determination of the cell size

Experience shows that a good rule of the thumb for the cell size happens to be $\Delta z = \lambda_{min}/10$.

$$\lambda_{min} = \frac{v_{min}}{f_{max}} = \frac{c_0}{f_{max} \cdot \sqrt{\varepsilon_{r\,max}}}$$

For the envisioned system, the value for f_{max} is given by the FCC limits [2] and it is 10.6 GHz. At this frequency, the tissues with the higher ε_r of the multilayer structure under analysis are the muscle and the heart, with a value $\varepsilon_r \approx 35$ [3]. Replacing and computing,

$$\lambda_{min} = \frac{3 \times 10^8 [\text{m/s}]}{10.6 \times 10^9 [\text{Hz}] \cdot \sqrt{35}} = 4.78 \times 10^{-3} [\text{m}]$$

Then, $\Delta z = \lambda_{min}/10 \approx 0.45$ [mm]

4   Layout of the multilayer structure

Fig. 2 shows the layout of a portion of the human chest near the heart and the source of UWB impulses. The chest is modeled as a multilayer structure composed of four semi-infinite layers of lossy and dispersive tissues that precede the heart.

The source is located 15 cm away from the air/skin interface because this was the maximum distance obtained in previous approximations of the same problem [4]; [5] and [6]. However, as is, this model do not account for the free space loss suffered by the pulse before it hits the air/skin interface. Therefore, the attenuation that will result from the simulation can be though as the attenuation due only to the propagation through the chest tissues.

The total number of cells required to simulate the region of interest is:

$$\#\text{cells} = \frac{\text{Region of interest}}{\text{cell size}} = \frac{200 \; [\text{mm}]}{0.45 \; [\text{mm}]} = 444.4 \cong 450 \; \text{cells}$$
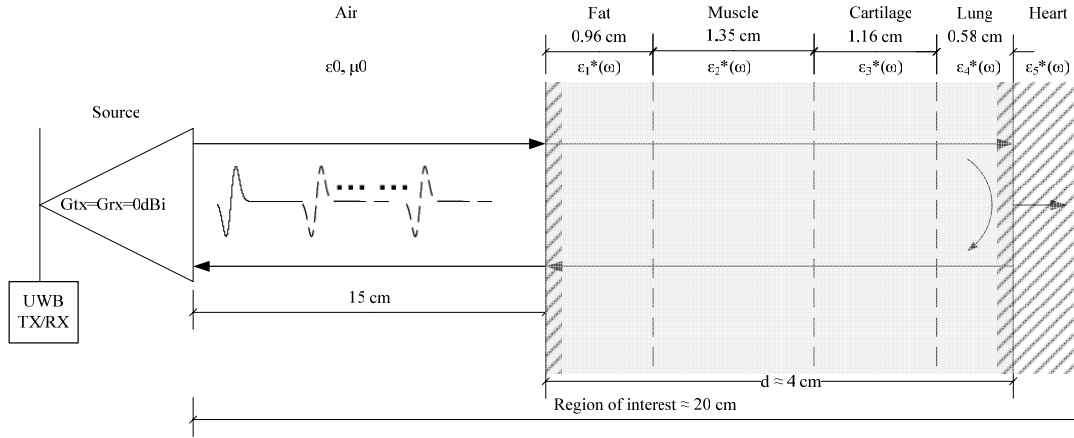
Fig. 2. Simplified model of the chest composed of 4 semi-infinite layers of lossy and dispersive tissue. The source is thought to be at around 15cm from the skin. The total region of interest includes one centimeter more to the right to account for the penetration of the wave into the heart.

5 One Dimensional Perfectly Matched Layer (PML)

To avoid unpredictable results into the region of interest, it is necessary to avoid the reflections coming from its boundaries implementing some kind of absorbing boundary conditions. Ref. [1] mentions several approaches to realize them. Here, it is adopted the Perfectly Matched Layer (PML) method, that creates a region neighboring the one of interest, in which the fields are heavily attenuated by means of fictitious dielectric and permeabilities constants. The total problem space will now be constituted by the region of interest plus the PML regions.

The idea is that if the impedance between the PML and the region of interest $\eta = \sqrt{\mu/\varepsilon}$ remains constant no reflection would occur. Also by making both μ and ε complex, one makes the PML region lossy, so the pulse will die out before it hits the problem space boundary.

Moving (1) to the frequency domain and adding the fictitious dielectric constant ε_F^* and the fictitious permeability μ_F^*, results:

$$j\omega \widetilde{D}x \cdot \varepsilon_F^*(z) = -c_0 \frac{\partial Hy}{\partial z} \tag{4}$$

$$\widetilde{D}x(\omega) = \varepsilon_r^*(\omega) \cdot \widetilde{E}x(\omega)$$

$$j\omega Hy \cdot \mu_F^*(z) = -c_0 \frac{\partial \widetilde{E}x}{\partial z} \tag{5}$$

In free space, the normalized units make $\eta_0 = 1$, so the PML condition imposes:

$$\eta_0 = \eta_F = \sqrt{\frac{\mu_F^*}{\varepsilon_F^*}} = 1 \tag{5a}$$

where μ_F^* and ε_F^* are two complex quantities of the form:

$$\varepsilon_F^* = \varepsilon_F + \frac{\sigma_D}{j\omega\varepsilon_0}$$

$$\mu_F^* = \mu_F + \frac{\sigma_H}{j\omega\mu_0} \tag{6}$$

Adopting $\varepsilon_F = \mu_F = 1$ and $\sigma_H/\mu_0 = \sigma_D/\varepsilon_0$, the value in Eq. (5a) becomes:

$$\eta_0 = \eta_F = \sqrt{\frac{\mu_F^*}{\varepsilon_F^*}} = \sqrt{\frac{1 + \sigma_D(z)/j\omega\varepsilon_0}{1 + \sigma_D(z)/j\omega\varepsilon_0}} = 1$$

If $\sigma_D(z)$ increases gradually as it goes into the PML, Eqs. (4) and (5) will cause $\widetilde{D}x$ and Hy to be attenuated. Using the values (6) together with the previous assumptions one can rewrite (4) and (5) as:

$$j\omega \cdot \left(1 + \frac{\sigma_D(z)}{j\omega\varepsilon_0}\right)\widetilde{D}x = -c_0 \frac{\partial Hy}{\partial z} \tag{7}$$

$$j\omega \cdot \left(1 + \frac{\sigma_D(z)}{j\omega\varepsilon_0}\right)Hy = -c_0 \frac{\partial \widetilde{E}x}{\partial z}$$

Starting with Eq. (7), before putting it into the FDTD formulation, its left side can be written as:

$$j\omega \cdot \left(1 + \frac{\sigma_D(z)}{j\omega\varepsilon_0}\right)\widetilde{D}x = j\omega\widetilde{D}x + \frac{\sigma_D(z)}{\varepsilon_0}\widetilde{D}x$$

Moving to the time domain and then taking the finite difference approximations one gets the following:

$$\frac{\partial \widetilde{D}x}{\partial t} + \frac{\sigma_D(z)}{\varepsilon_0}\widetilde{D}x \cong \frac{\widetilde{D}_x^{n+1/2}(k) - \widetilde{D}_x^{n-1/2}(k)}{\Delta t} + \frac{\sigma_D(k)}{\varepsilon_0}\frac{\widetilde{D}_x^{n+1/2}(k) - \widetilde{D}_x^{n-1/2}(k)}{2} =$$

$$= \widetilde{D}_x^{n+1/2}(k)\frac{1}{\Delta t}\left[1 + \frac{\sigma_D(k)\cdot\Delta t}{2\varepsilon_0}\right] - \widetilde{D}_x^{n-1/2}(k)\frac{1}{\Delta t}\left[1 - \frac{\sigma_D(k)\cdot\Delta t}{2\varepsilon_0}\right]$$

Replacing into (7) along with the spatial derivatives one gets:

$$\widetilde{D}_x^{n+1/2}(k)\frac{1}{\Delta t}\left[1 + \frac{\sigma_D(k)\cdot\Delta t}{2\varepsilon_0}\right] - \widetilde{D}_x^{n-1/2}(k)\frac{1}{\Delta t}\left[1 - \frac{\sigma_D(k)\cdot\Delta t}{2\varepsilon_0}\right] = -c_0 \frac{H_y^n(k+1/2) - H_y^n(k-1/2)}{\Delta z}$$

As stated before:

$$\frac{1}{\sqrt{\mu_0\varepsilon_0}}\frac{\Delta t}{\Delta z} = c_0 \cdot \frac{\Delta z/(2\cdot c_0)}{\Delta z} = \frac{1}{2}$$

So,

$$\widetilde{D}_x^{n+1/2}(k)\cdot\left[1 + \frac{\sigma_D(k)\cdot\Delta t}{2\varepsilon_0}\right] - \widetilde{D}_x^{n-1/2}(k)\cdot\left[1 - \frac{\sigma_D(k)\cdot\Delta t}{2\varepsilon_0}\right] = -\frac{1}{2}\left[H_y^n(k+1/2) - H_y^n(k-1/2)\right]$$

Solving for $\widetilde{D}_x^{n+1/2}(k)$:

$$\widetilde{D}_x^{n+1/2}(k) = \frac{1 - \frac{\sigma_D(k)\cdot\Delta t}{2\varepsilon_0}}{1 + \frac{\sigma_D(k)\cdot\Delta t}{2\varepsilon_0}}\widetilde{D}_x^{n-1/2}(k) - \frac{1}{2}\cdot\frac{1}{1 + \frac{\sigma_D(k)\cdot\Delta t}{2\varepsilon_0}}\left[H_y^n(k+1/2) - H_y^n(k-1/2)\right]$$

Defining the parameters:

$$gi2(k) = \frac{1}{1 + \sigma_D(k)\cdot\Delta t/(2\varepsilon_0)}$$

$$gi3(k) = \frac{1 - \sigma_D(k)\cdot\Delta t/(2\varepsilon_0)}{1 + \sigma_D(k)\cdot\Delta t/(2\varepsilon_0)}$$

One can write:

$$\widetilde{D}_x^{n+1/2}(k) = gi3(k)\cdot\widetilde{D}_x^{n-1/2}(k) - \frac{1}{2}\cdot gi2(k)\cdot\left[H_y^n(k+1/2) - H_y^n(k-1/2)\right]$$

Operating analogously on Hy:

$$H_y^{n+1}(k+1/2) = fi3(k+\frac{1}{2})\cdot H_y^n(k+1/2) - \frac{1}{2}fi2(k+\frac{1}{2})\cdot\left[\widetilde{E}_x^{n+1/2}(k+1) - \widetilde{E}_x^{n+1/2}(k)\right]$$

where

$$fi2(k+1/2) = \frac{1}{1 + \sigma_D(k+1/2)\cdot\Delta t/(2\varepsilon_0)}$$

$$fi3(k+1/2) = \frac{1 - \sigma_D(k+1/2)\cdot\Delta t/(2\varepsilon_0)}{1 + \sigma_D(k+1/2)\cdot\Delta t/(2\varepsilon_0)}$$

To calculate the parameter f and g, instead of varying the conductivities, an auxiliary parameter is used:

$$xn = \frac{\sigma\cdot\Delta t}{2\varepsilon_0}$$

that increases as it goes into the PML with the following expression suggested by [1]

$$xn(i) = \texttt{PML\_ATT\_FACTOR}\cdot\left(\frac{i}{pml\_length}\right)^3 \quad i = 1, 2, ..., pml\_length$$

where the cubic and the `PML_ATT_FACTOR` are just empirical numbers. For example, Ref. [1] recommends a `PML_ATT_FACTOR = 0.333`, however in this work, it was varied obtaining also good results with higher values such as 0.8.

The f and g parameters are then calculated as:

$$gi2(i) = \frac{1}{1+xn(i)} \qquad fi2(i+1/2) = \frac{1}{1+xn(i+1/2)}$$

$$gi3(i) = \frac{1-xn(i)}{1+xn(i)} \qquad fi3(i+1/2) = \frac{1-xn(i+1/2)}{1+xn(i+1/2)} \qquad i = 1, 2, ..., pml\_length$$

Within the region of interest, f and g are set to 1; whereas, throughout the PML, $gi2$ and $fi2$ will decrease from approximately 1 to $(1+$`PML_ATT_FACTOR`$)^{-1}$ (i.e. from 1 to 0.55 for `PML_ATT_FACTOR = 0.8`). The same will happen for $gi3$ and $fi3$ (i.e. from 1 to 0.11 for `PML_ATT_FACTOR = 0.8`). These values assure a smooth transition from the region of interest to the PML.

With the inclusion of a PML of 40 cells at both sides, the total problem space expressed in FDTD cells (one cell = 0.45mm) is depicted in Fig. 3.
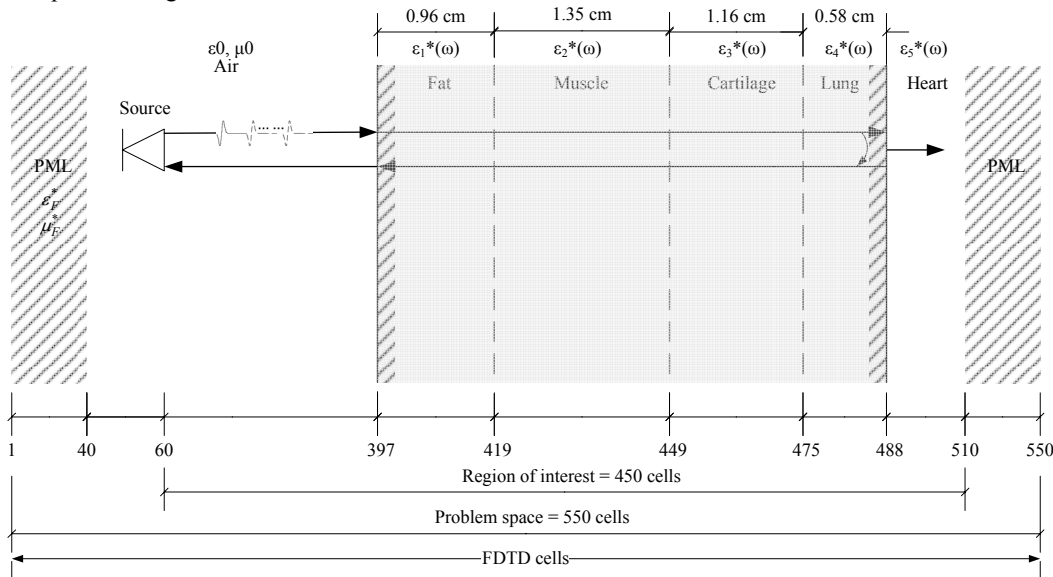

Fig. 3. FDTD cell layout of the simplified model of the chest containing two PML regions to act as absorbing boundaries in order to prevent unwanted reflections into the region of interest.

Although this PML formulation has been thought for free space, it works very well also for the other media involved in this problem, as it will be shown later in the validations.

6 Source impulse model

Typically, the envisioned UWB communications devices use pulses with a shape that has the form of some derivative of a Gaussian pulse. For the sake of this work, it is followed the approach adopted by Time Domain Corporation, one of the pioneers manufacturers of UWB equipment [7]. Time domain declares that their PulsON® technology emit ultra-short "Gaussian" monocycles [8]. The literature knows the Gaussian monocycles as the first derivative of a Gaussian pulse. So, if a Gaussian pulse has the form:
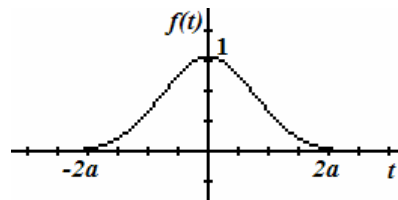
$$f(t) = e^{-\left(\frac{t}{a}\right)^2}$$

Fig. 4. Gaussian pulse

the Gaussian monocycle is

$$p(t) \propto t e^{-\left(\frac{t}{a}\right)^2}$$

Using $kp = \sqrt{2}/a \cdot e^{1/2}$ as the proportionality constant to make the amplitude = 1, the impulse used as a source becomes:

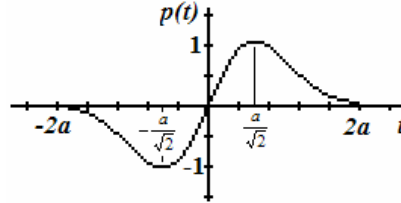$$p(t) = kp \cdot t \cdot e^{-\left(\frac{t}{a}\right)^2}$$

Fig. 5. Gaussian monocycle

The spectrum of this Gaussian monocycle is given by Fourier transforming *p(t)*

$$P(f) = F[p(t)] = \frac{1}{2} kp \cdot a^3 \cdot \pi \sqrt{\pi} \cdot f \cdot e^{-(\pi a f)^2}$$
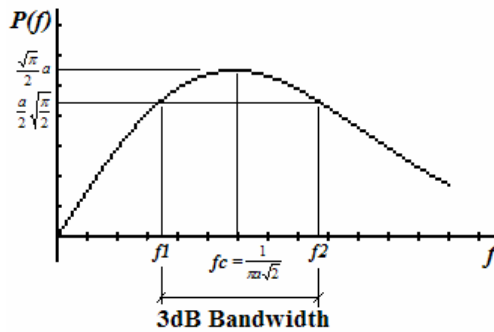

Fig. 6. Frequency spectrum of the Gaussian monocycle

The specifications of the P210 Evaluation Kit mentions that the radiated center frequency is approximately $fc = 4.7$ GHz, therefore:

$$a = \frac{1}{\pi\sqrt{2} \cdot fc} = \frac{1}{\pi\sqrt{2} \cdot 4.7 \times 10^9} \cong 50 \ [ps]$$

According to Fig. 5, the Gaussian monocycle that will be used for the simulations will have a duration of 4a = 0.2 [ns]. Such a pulse, has a 3dB bandwidth ≈ 5.2 GHz (i.e. *f1* = 2.2GHz, *f2* = 7.4 GHz), which makes it inherently ultra-wide band.

7 Validations of the formulation

Before going ahead further in the modeling it will be nice to validate the FDTD formulation made so far against some basic analytical solutions to be sure that the developed C program is working as expected.

7.1 Verification of the time of flight of the impulse over the multilayer structure when considered lossless.

The most trivial verification is to calculate the theoretical time it takes for the pulse to travel from the source to the heart wall and compare it with simulations results.
Since the frequency dependence of the tissues has not been modeled yet, the constitutive parameters are taken at 4GHz. This will make the results only approximate, but good enough to check if the program is working correctly.
TABLE I shows the time it takes for a 4 GHz wave originated at the source to hit the heart wall when the multilayer structure is considered lossless.

TABLE I

TABLE I

TRAVEL TIME OF A 4GHZ WAVE FROM THE SOURCE UNTIL IT HITS THE HEART WALL

Cartilage	ε_r at 4GHz [9]	Δz		$\Delta t=\sqrt{\varepsilon_r}\cdot\Delta z/c_0$ [ps]
		Thickness [FDTD cells]	Thickness [mm] (1cell=0.45mm)	
Air (free space)	1.0	337	151.65	505.85
Fat	5.5	22	9.90	77.45
Muscle	50.0	30	13.50	318.42
Cartilage	35.0	26	11.70	230.89
Lung	20.0	13	5.85	87.27
TOTAL (one way)				1219.87

Considering that in the program the implementation of the pulse is shifted 200 [ps], then the first maximum of the pulse should hit the heart wall at: $t = 1219.87 + \left(200 - a/\sqrt{2}\right) \cong 1385$ [ps]

By running the simulation it was obtained $t \approx 1397$ [ps]. The small difference is due to the interaction of the reflected part of the wave that already penetrated the heart wall which briefly delays the arrival of the maximum from the theoretical value that, as such, do not consider the reflections. Fig. 7 shows the results of the simulation.
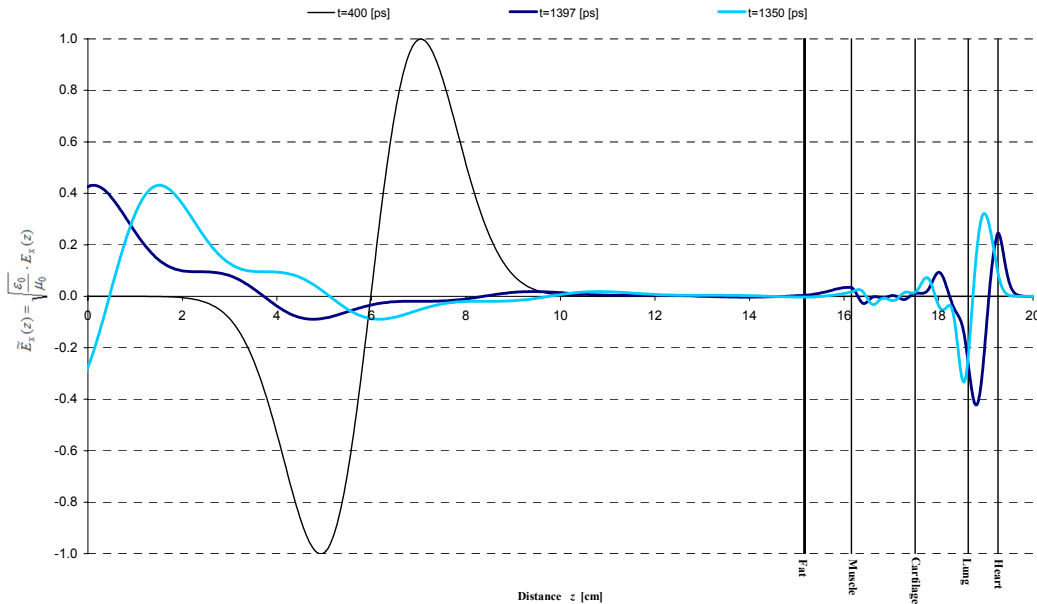
Fig. 7. Simulation of Gaussian monocycle impinging multiple layers of lossless tissues. At 400 [ps] the pulse is travelling on free space. Later on its shape is being altered by the multiple reflections suffered into the multilayer structure. At 1397 [ps] the maximun hits the heart wall.

Another value to validate is the total transmission coefficient. The transmission coefficients at 4 GHz as calculated in [4] are: T1=0.60; T2=0.50; T3=1.09; T4=1.14; and T5=0.75 respectively for each of the boundaries of Fig. 2. Thus, the total

transmission coefficient for the multilayer structure is $T = \prod_{i=1}^{5} T_i \cong 0.2796$.

Running the simulation for 1350 [ps] (i.e. long enough to let the impulse penetrate into the heart but short enough to minimize the influence of the reflections), and measuring the value of the field near to the boundary one gets:

$$\widetilde{E}_x(z = 19.305\,\text{cm}) = 5.61\times10^{-2}\left[\text{V}/(\Omega\cdot\text{m})\right]$$

At this point the time that has passed since the beginning of the impulse penetrated the heart wall is:

$$\Delta t = \frac{\Delta z}{v} = \frac{(19.66 - 19.305)\times10^{-2}\,[\text{m}]}{c_0/\sqrt{55}} \cong 86.66 \ [\text{ps}]$$

Computing the value of the incident impulse at free space for the same time interval gives: $p(t = 86.66 \times 10^{-12}) = 200.4 \times 10^{-3}$, so the transmission coefficient of the structure can be approximated as $56.1/200.4 \approx 0.279$, which is also very near to the theoretical value considering the approximation. Fig. 7 also shows the propagation of the pulse up to 1350 [ps].

8

7.2 Verification of the intensity impinging the heart wall at 4GHz considering the structure lossy but still non dispersive.

The tissues under study present the following conductivities at 4GHz:

Media	σ [S/m]
air	0.00
fat	0.25
Muscle	3.50
Cartilage	3.00
Lung	1.50
Heart	4.00

Fig. 8 shows the results. As expected the maximum hits the heart wall at approximately 1397 [ps]. The value is: 1.384 x 10^{-2}.

Going ahead with the simulation the maximum of the reflection coming back from the heart would reach the source antenna after 2782 [ps], with a value of 2.463 x 10^{-4}. Given that the source impulse has unit amplitude this value gives directly the round trip attenuation introduced by the lossy multilayer structure. In dB the value is: 20·log 2.463 x 10^{-4} ≈ -72.17 dB. This attenuation is very near the 71.79 dB calculated analytically in [10], which validates the result. Fig. 9 shows the shape of the returning pulse after 2782 [ps] when the maximum hits the source antenna located at position 0 [cm].
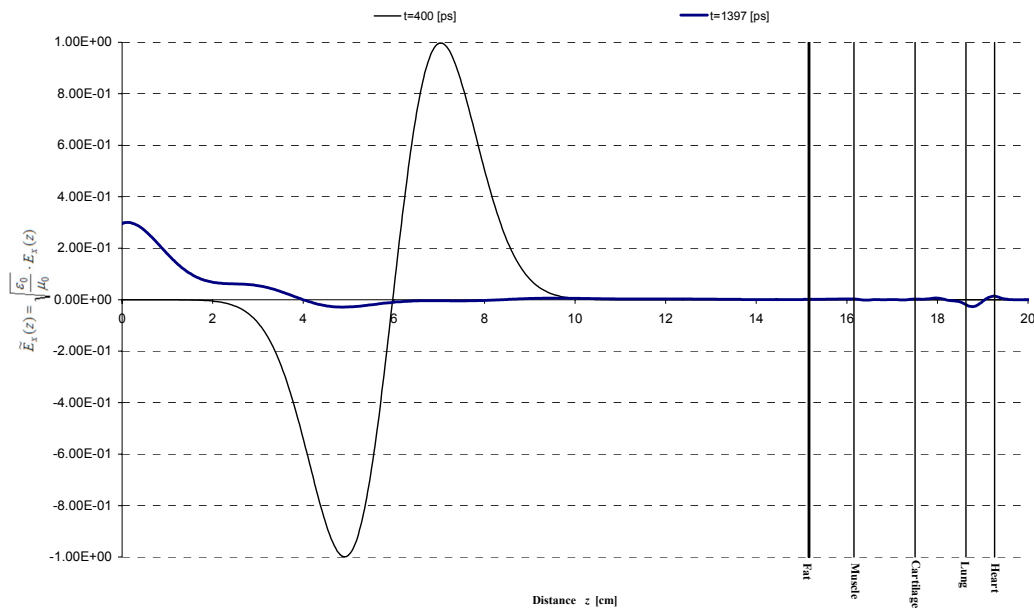

Fig. 8. Simulation of Gaussian monocycle impinging multiple layers of lossy tissues. At 400 [ps] the pulse is travelling on free space where σ = 0. After approximately 1397 [ps], the maximun hits the heart wall after being heavily attenuated by the media.
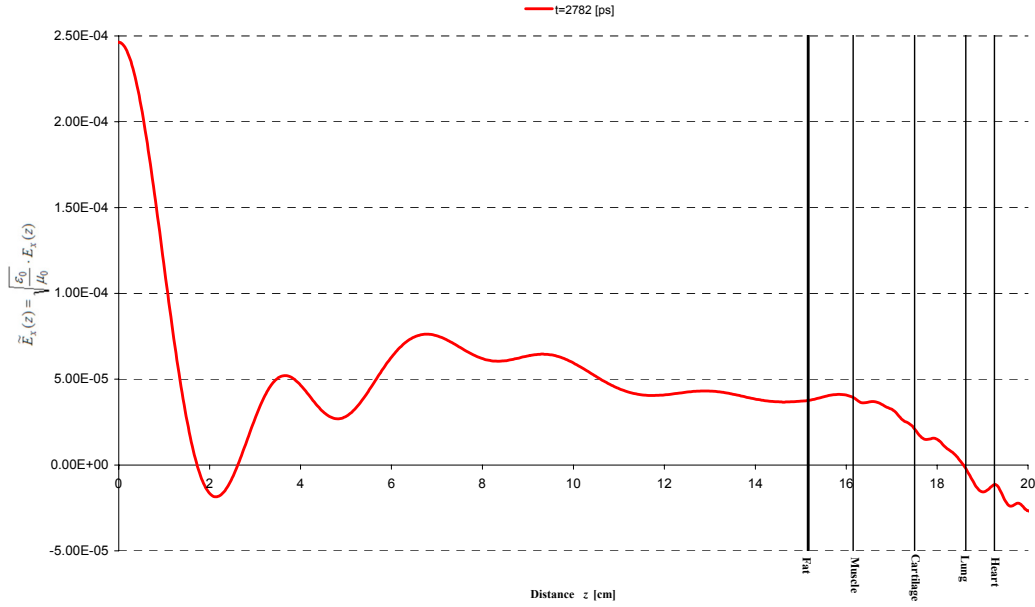
Fig. 9. Simulation of Gaussian monocycle impinging multiple layers of lossy tissues. After 2782 [ps] the maximun returns to the source antenna for detection. The round trip attenuation at 4GHz is approximately 72 dB.

8 Modeling multiple layers of frequency-dependent media

So far, the multilayer structure has been modeled as lossy but not considering its frequency dispersion characteristics. The dispersion of the tissues is of fundamental interest for the sake of this work because having an UWB impulse source, one may well suppose that if its frequency components are attenuated differently, the total attenuation of the whole pulse should be less than the value calculated previously, thanks to the contribution of lower frequencies. This in turn will improve the range, something that is highly desirable for a contactless sensor such as the one envisioned here.

Gabriel et al. proposed a 4 Cole-Cole model to represent the frequency dependence of the complex permittivities of the tissues [3]:

$$\varepsilon_r^*(\omega) = \varepsilon_\infty + \frac{\sigma_i}{j\omega\varepsilon_0} + \sum_{m=1}^{4} \frac{\Delta\varepsilon_m}{1 + (j\omega\tau_m)^{1-\alpha_m}}$$

where

$\varepsilon_r^*(\omega)$: Complex relative permittivity

ε_∞ : Permittivity at field frequencies $\omega\tau \gg 1$

$\Delta\varepsilon_m = \varepsilon_s - \varepsilon_\infty$: Magnitude of the dispersion region

ε_s : Permittivity at $\omega\tau \ll 1$

τ_m : Time constant of each relaxation region

α_m : Measure of the broadening of the dispersion

σ_i : Static ionic conductivity

For the tissues under consideration these values are:

TABLE III
CONSTITUTIVE PARAMETERS FOR THE 4 COLE-COLE MODEL OF GABRIEL ET AL.[3]

Media	ε_∞	$\Delta\varepsilon_1$	$\Delta\varepsilon_2$	$\Delta\varepsilon_3$	$\Delta\varepsilon_4$	τ_1 [ps]	τ_2 [ns]	τ_3 [µs]	τ_4 [ms]	σ_i	α_1	α_2	α_3	α_4
Breast fat	2.5	3	15	5×10^{-4}	2×10^{-7}	17.68	63.66	454.7	13.26	0.01	0.1	0.1	0.1	0
Muscle	4	50	7000	1.2×10^{-6}	2.5×10^{-7}	7.23	353.68	318.31	2.274	0.2	0.1	0.1	0.1	0
Cartilage	4	38	2500	1×10^{-5}	4×10^{-7}	13.263	144.686	318.31	15.915	0.15	0.15	0.15	0.1	0
Lung (inflated)	2.5	18	500	2.5×10^{-5}	4×10^{-7}	7.96	63.66	159.15	7.958	0.03	0.1	0.1	0.2	0
Heart	4	50	1200	4.5×10^{-5}	2.5×10^{-7}	7.96	159.15	72.34	4.547	0.05	0.1	0.05	0.22	0

The Cole-Cole terms proposed by Gabriel et al. makes its FDTD implementation particularly cumbersome. However, noticing that the values of α_m are in general $\ll 1$, one can consider the distribution parameter $\alpha_m \cong 0$ and simplify the formulation using 4 Debye terms, resulting in:

$$\varepsilon_r^*(\omega) = \varepsilon_\infty + \frac{\sigma_i}{j\omega\varepsilon_0} + \sum_{m=1}^{4} \frac{\Delta\varepsilon_m}{1 + j\omega\tau_m}$$

which, even though is not as accurate as the previous, gives equally satisfactory results and simplifies a lot the formulation of the problem.

Using the electric flux density one can write:

$$\widetilde{\mathbf{D}}(\omega) = \left[\varepsilon_\infty + \frac{\sigma_i}{j\omega\varepsilon_0} + \sum_{m=1}^{4} \frac{\Delta\varepsilon_m}{1 + j\omega\tau_m} \right] \cdot \widetilde{\mathbf{E}}(\omega)$$

Going into the Z domain

$$\widetilde{\mathbf{D}}(z) = \varepsilon_\infty \cdot \widetilde{\mathbf{E}}(z) + \frac{\sigma_i \cdot \Delta t/\varepsilon_0}{1 - z^{-1}} \cdot \widetilde{\mathbf{E}}(z) + \widetilde{\mathbf{E}}(z) \cdot \sum_{m=1}^{4} \frac{\Delta\varepsilon_m \cdot \Delta t/\tau_m}{1 + e^{-\Delta t/\tau_m} \cdot z^{-1}} \tag{8}$$

The following auxiliary parameters are defined:

$$I(z) = \frac{\sigma_i \cdot \Delta t/\varepsilon_0}{1 - z^{-1}} \cdot \widetilde{\mathbf{E}}(z) = z^{-1} I(z) + \frac{\sigma_i \cdot \Delta t}{\varepsilon_0} \widetilde{\mathbf{E}}(z)$$

$$S_m(z) = \frac{\Delta\varepsilon_m \cdot \Delta t/\tau_m}{1 + e^{-\Delta t/\tau_m} \cdot z^{-1}} \widetilde{\mathbf{E}}(z) = e^{-\Delta t/\tau_m} \cdot z^{-1} \cdot S_m(z) + \frac{\Delta\varepsilon_m \cdot \Delta t}{\tau_m} \widetilde{\mathbf{E}}(z) \qquad \text{for } m = 1, 2, 3, 4$$

$$S(z) = \sum_{m=1}^{4} e^{-\Delta t/\tau_m} \cdot z^{-1} \cdot S_m(z) + \frac{\Delta\varepsilon_m \cdot \Delta t}{\tau_m} \widetilde{\mathbf{E}}(z)$$

So, Eq. (8) becomes:

$$\widetilde{\mathbf{D}}(z) = \varepsilon_\infty \cdot \widetilde{\mathbf{E}}(z) + z^{-1} I(z) + \frac{\sigma_i \cdot \Delta t}{\varepsilon_0} \widetilde{\mathbf{E}}(z) + \sum_{m=1}^{4} e^{-\Delta t/\tau_m} \cdot z^{-1} \cdot S_m(z) + \widetilde{\mathbf{E}}(z) \cdot \sum_{m=1}^{4} \frac{\Delta\varepsilon_m \cdot \Delta t}{\tau_m}$$

Solving for $\widetilde{\mathbf{E}}(z)$:

$$\widetilde{\mathbf{E}}(z) = \frac{\widetilde{\mathbf{D}}(z) - z^{-1} I(z) - \sum_{m=1}^{4} e^{-\Delta t/\tau_m} \cdot z^{-1} \cdot S_m(z)}{\varepsilon_\infty + \frac{\sigma_i \cdot \Delta t}{\varepsilon_0} + \sum_{m=1}^{4} \frac{\Delta\varepsilon_m \cdot \Delta t}{\tau_m}}$$

Going to back to the sampled time domain: $\widetilde{\mathbf{E}}(z) \to E^n$; $z^{-1} \cdot \widetilde{\mathbf{E}}(z) \to E^{n-1}$ where n is the time counter such that the total simulated time is $t = n \cdot \Delta t$ being Δt the time step. Then,

$$E^n = \frac{D^n - I^{n-1} - \sum_{m=1}^{4} e^{-\Delta t/\tau_m} \cdot S_m^{n-1}}{\varepsilon_\infty + \frac{\sigma_i \cdot \Delta t}{\varepsilon_0} + \sum_{m=1}^{4} \frac{\Delta\varepsilon_m \cdot \Delta t}{\tau_m}}$$

where

$$I^n = I^{n-1} + \frac{\sigma_i \cdot \Delta t}{\varepsilon_0} E^n$$

$$S_m^n = e^{-\Delta t/\tau_m} \cdot S_m^{n-1} + \frac{\Delta\varepsilon_m \cdot \Delta t}{\tau_m} E^n \qquad \text{for } m = 1, 2, 3, 4$$

The FDTD computer code becomes:

```
dx[k] and hy[k] Remain the same
ex[k] = ga[k] * (dx[k] - ix[k] - del_exp1[k]*sx1[k] - del_exp2[k]*sx2[k] -
                                 del_exp3[k]*sx3[k] -
                                 del_exp4[k]*sx4[k]);

ix[k] = ix[k] + gb[k]*ex[k];
sx1[k]= del_exp1[k]*sx1[k] + gc1[k]*ex[k];
sx2[k]= del_exp2[k]*sx2[k] + gc2[k]*ex[k];
```

```
sx3[k]= del_exp3[k]*sx3[k] + gc3[k]*ex[k];
sx4[k]= del_exp4[k]*sx4[k] + gc4[k]*ex[k];
ga[k] = 1.0/(epsilon[k] + sigma[k]*dt/epsz + delta_epsilon1[k]*dt/tau1[k] +
                                            delta_epsilon2[k]*dt/tau2[k] +
                                            delta_epsilon3[k]*dt/tau3[k] +
                                            delta_epsilon4[k]*dt/tau4[k] );
gb[k] = sigma[k]*dt/epsz;
gc1[k] = delta_epsilon1[k]*dt/tau1[k];
gc2[k] = delta_epsilon2[k]*dt/tau2[k];
gc3[k] = delta_epsilon3[k]*dt/tau3[k];
gc4[k] = delta_epsilon4[k]*dt/tau4[k];
del_exp1[k] = exp(-dt/tau1[k]);
del_exp2[k] = exp(-dt/tau2[k]);
del_exp3[k] = exp(-dt/tau3[k]);
del_exp4[k] = exp(-dt/tau4[k]);
```

9   Simulation results

Incorporating the dispersive and lossy formulation into the program and running the simulation, the results are shown in Fig. 10.
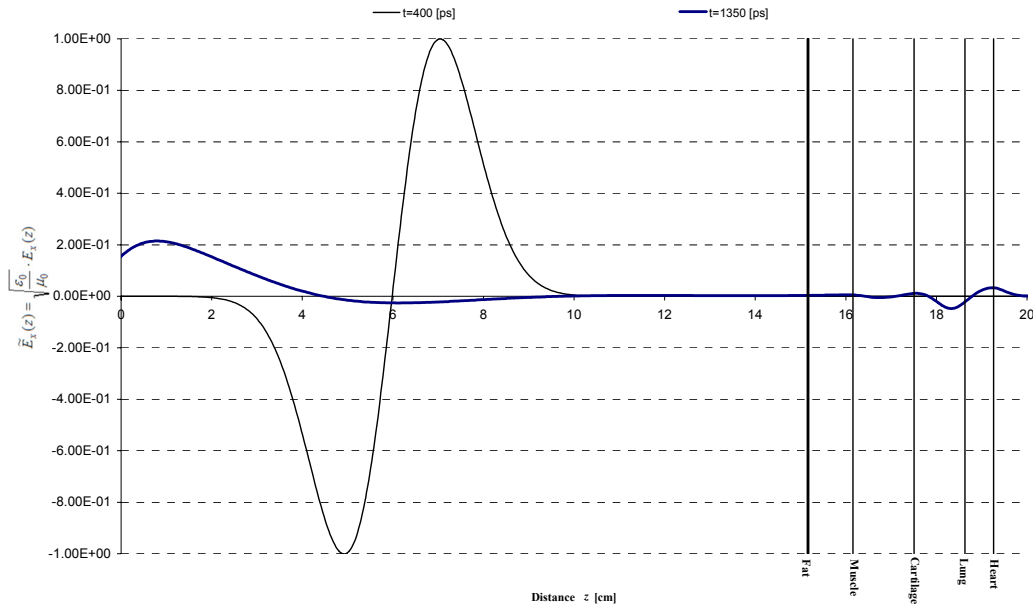
Fig. 10. Simulation of Gaussian monocycle impinging multiple layers of lossy tissues and dispersive tissues. After 1350 [ps] hits the heart wall. The one way attenuation is approximately 29.5 dB.

The impulse hits the heart wall at approximately 1350 [ps] with a value of 3.338×10^{-2}. As expected the impulse gets less attenuated due to the influence of the lower frequency components which are in turn less attenuated, because the conductivity decreases with frequency. On the other hand the impulse travels faster because the higher frequencies components of the impulse are in turn traveling faster, because the permittivity of the tissues decreases as the frequency increases.

Fig. 11 shows the reflected impulse after 2500 [ps]. As expected it has widen to nearly 0.5 [ns], however its shape has not been distorted too much, which makes it easily detectable with a correlation receiver. The attenuation has also improved a lot. Considering the value of the positive maximum (worst case), the round trip attenuation is: $20 \cdot \log 7.83 \times 10^{-3} \approx 42$ dB. This huge improvement of nearly 30 dB compared with the previous value computed only at 4 GHz, shows the advantage of using UWB impulse sensing instead other monofrequency techniques.
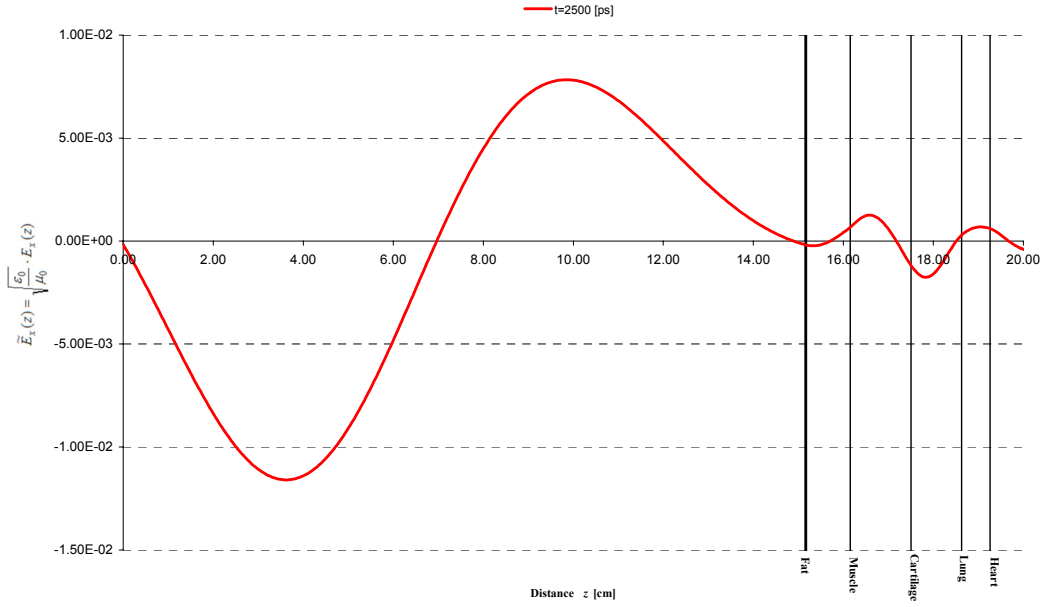
Fig. 11. Simulation of Gaussian monocycle impinging multiple layers of lossy tissues and dispersive tissues after 2500 [ps]. The figure shows the expected widenning of the returning impulse.

According to Fig. 11, a sensing system working as a monostatic gated impulse radar positioned at 15 [cm] from the chest, would have to transmit the impulse and switch off the transmitter after approximately 0.4 [ns]. Then, it should turn on the receiver after 2.5 [ns] for approximately 0.5 [ns], to detect the reflection. Fig. 12, shows in detail the evolution over time of $\widetilde{E}_x(z = 0\,\text{cm})$.
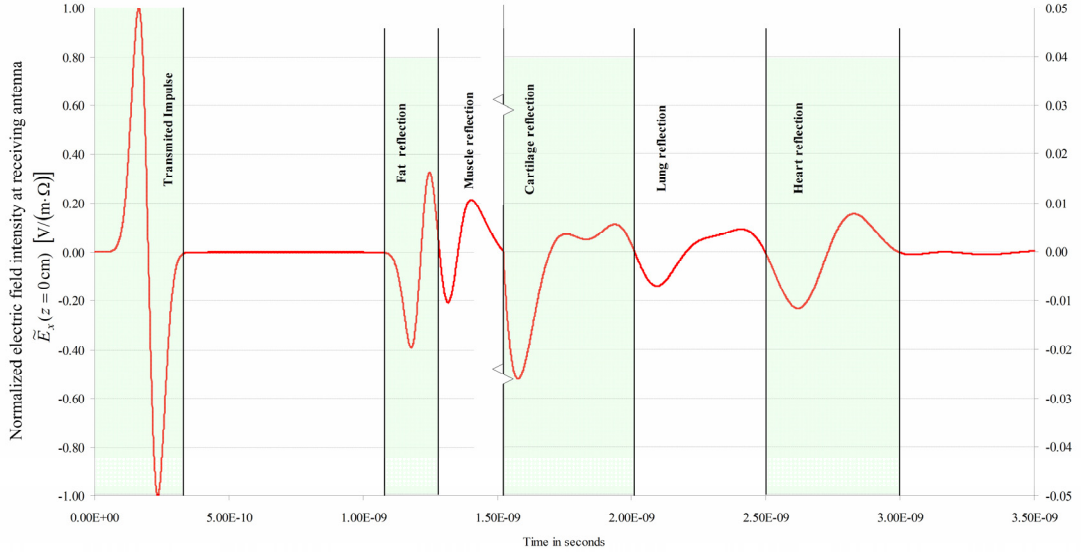
Fig. 12. Magnitude of the normalized electric field versus time at the receiving antenna position (0 cm). The different regions indicate the reflections received from the different layers of tissue. The scale of the ordinates change between muscle and cartilage for a better reading.

Checking for the feasibility of such a system using the previously mentioned UWB evaluation kit from Time Domain Corporation; one gets that the peak transmitted power Ptmax can be approximated as:

$$Ptmax = \frac{EIRP}{\tau \cdot PRF} = \frac{52.48 \times 10^{-6}\,[\text{W}]}{212.8 \times 10^{-12}\,[\text{s}] \cdot 9.6 \times 10^{6}\,[\text{Hz}]} = 25.69\ [\text{mW}] \cong 14\,\text{dBm}$$

where the data, as taken from its data sheet [7], are:

13

EIRP: Effective Isotropic Radiated Power = -12.8 dBm
τ: Gaussian monocycle impulse width 1/*fc*
fc: Center frequency (radiated) approx. 4.7 GHz
PRF: Pulse Repetition Frequency 9.6 MHz.

The attenuation value as given by the simulation is:

$$L = \frac{P_r}{P_i} = \frac{S_r}{S_i} = \frac{E_r^2}{E_i^2} = \frac{\widetilde{E}_r^2}{\widetilde{E}_i^2} = \left(\frac{\widetilde{E}_r}{\widetilde{E}_i}\right)^2$$

$$L_{dB} = 10\log\left(\frac{\widetilde{E}_r}{\widetilde{E}_i}\right)^2 = 20\log\left(\frac{\widetilde{E}_r}{\widetilde{E}_i}\right) = 20\log\frac{7.83\times10^{-3}}{1} \cong 42\,\text{dB}$$

where the suffixes *r* and *i* indicates reflected and incident power respectively, and *S* is the power density in W/m^2.
Therefore the reflected power which in this case coincides with the received power[1], is:

$$P_r[\text{dBm}] = P_i[\text{dBm}] + L[\text{dB}] = 14 - 42 = -28[\text{dBm}]$$

Since the receiver sensitivity P_r^{min} for QFTM4 modulation at 600 kbps is approximately -100[dBm] [11], there is still a lot of room to stand higher losses and/or increase the sensing distance, hopefully reaching the desirable range of one meter.

10   Conclusions

These FDTD simulations results constitute a step forward in the state of the art of vital signs monitoring using UWB radar technology. Previous publications predicted the performance either empirically, by using test hardware, or analytically by approximating the results using the traditional radar expressions for far field formulation. The former lacked insight about the phenomenology of the process and the latter did not account for the UWB characteristics of the impulses used. This work confirms the goodness of using UWB impulses to withstand the heavy attenuations introduced by the chest tissues compared with a monofrequency approach.

As a future work remains the modeling in 3D and the study of the scattering characteristics of the heart, that here was considered as a semi-infinite media which is not exactly the case because its dimensions are not much higher than λ.

References

[1]   Sullivan, D. M.; "Electromagnetic simulation using the FDTD method"; *IEEE press series on RF and microwave technology*; New York; 2000.

[2]   Federal Communications Commission; "Revision of Part 15 of the Commission's Rules Regarding Ultra-Wideband Transmission Systems"; ET Docket 98-153; Washington, D.C., U.S.A; April 22, 2002.

[3]   S.Gabriel, R.W.Lau and C.Gabriel: "The dielectric properties of biological tissues: III. Parametric models for the dielectric spectrum of tissues", *Phys. Med. Biol.* 41 (1996), 2271-2293.

[4]   Bilich, C. G.; "Feasibility of Dual UWB Heart Rate Sensing and Communications under FCC power restrictions"; *Third International Conference on Wireless and Mobile Communications, ICWMC 2007*; March 4-9, 2007 - Guadeloupe, French Caribbean; accepted for publication.

[5]   Bilich, C. G.; "Bio-Medical Sensing using Ultra Wideband Communications and Radar Technology: A Feasibility Study". *FIRST INTERNATIONAL CONFERENCE ON PERVASIVE COMPUTING TECHNOLOGIES FOR HEALTHCARE 200*6, IEEE, CREATE-NET, ICST, Innsbruck, Austria, 29/11 ~ 1/12, 2006.

[6]   Bilich, C. G.; "Bio-Medical Sensing using Ultra Wideband Communications and Radar Technology"; *PhD Proposal*, submitted for the 20th Cycle of the Program in Information and Communications Technologies; Department of Information and Telecommunications Technology; University of Trento; Italy; January 2006. Available: http://eprints.biblio.unitn.it/archive/00001045/

[7]   Time Domain Corporation, *"P210 Evaluation kit: Fostering Ultra-Wideband Innovation and Integration"*. [Online] last accessed: 07/31/2006. Available: http://www.timedomain.com/products/P2101EVK.pdf

[8]   ---, *"PulsON® Technology Overview"*; Huntsville, AL, USA; July 2001. [Online] last accessed: 07/31/2006. Available: http://www.timedomain.com

[9]   S.Gabriel, R.W.Lau and C.Gabriel: "The dielectric properties of biological tissues: II. Measurements in the frequency range 10 Hz to 20 GHz", *Phys. Med. Biol.* 41 (1996), 2251-2269.

---

[1] This is not taking into account that in reality (i.e. three dimensions) the E field attenuates as the square of the distance as it propagates, which will be the subject of a future simulation in 3D.

[10] Bilich, C. G; "*UWB radars for Bio-Medical Sensing: Attenuation Model for Wave Propagation in the Body at 4GHz*"; Technical Report DIT-06-051, Informatica e Telecomunicazioni, University of Trento, Aug. 2006. Available: http://eprints.biblio.unitn.it/archive/00001049/01/TechRep_UWB_AttModel.pdf

[11] Time Domain Corporation; *"System Analysis Module User's Manual: PulsON 210 UWB Reference Design"*; P210-320-0102B; page 75; December 2005.